STABLE ROBOTIC GRASP SYNTHESIS ON A SPENT ROCKET STAGE FOR ON-ORBIT CAPTURING

Virtual Conference 19–23 October 2020

Nikos Mavrakis[1], Yang Gao[1]

[1]STAR-LAB, Surrey Space Centre, University of Surrey, United Kingdom, E-mail: n.mavrakis@surrey.ac.uk
[1]STAR-LAB, Surrey Space Centre, University of Surrey, United Kingdom, E-mail: yang.gao@surrey.ac.uk

ABSTRACT

This paper describes a novel approach on orbital target capturing of a spent Apogee Kick Motor (AKM), by using robotic finger contact stability analysis similarly to terrestrial robotics. The surface curvature of the nozzle offers a robust candidate contact point. The stability of the grasp is assessed according to the Intrinsic Stiffness Matrix of the grasp and the mass matrix of the target, which are expressed on a common coordinate frame, multiplied, and the minimum eigenvalue of the product serves as a stability criterion. We perform a quantitative analysis to assess the stability over variations of the grasping parameters. We also execute a simulation of a chasing spacecraft equipped with a robot manipulator and gripper, grasping an AKM and pulling it towards its body. The results suggest that the grasp is stable, and the finger displacement from the grasped surface is negligible. The results from this paper can be used to develop autonomous stable grasp planning algorithms for orbital robotics.

1 INTRODUCTION

Robots are becoming increasingly deployed in space applications, executing tasks with various levels of autonomy. In orbital robotics, on-orbit servicing and space debris removal are two growing fields that will call for further use of robotic arms. The main usage for the manipulators was for docking and berthing with cooperative targets, or capturing an uncooperative target. Docking usually requires a matching mechanical interface on the robot arm and the target, and numerous interfaces have been developed for this purpose [1]. An interface may not always be present, especially in an uncooperative target and this calls for the design of more elaborate capturing methods using other mechanisms such as harpoons, nets ea. [2]. In such a case, other parts of the spacecraft need to be used as capturing points. Early robotic missions, such the ETS-VII used handles grasped by robotic clamps, and detected the handle position with visual markers [3]. Handle grasping has also been demonstrated on the International Space Station by a small free-flying robot [4]. Some works proposed the use of the *Payload Attachment Fixture* (PAF) of a spacecraft as a grasping point, a ring-like extrusion on the spacecraft used for mounting on the launch vehicle [5-7]. Another potential component for contact is an engine nozzle. It can be used primarily for deorbiting *Apogee Kick Motors* (AKMs) i.e. rocket propulsion stages responsible for placing a launched satellite in its final orbit. Typically, an expanding probe is inserted in the AKM throat, trapping it after contact [8-10]. In [11] the authors conducted a feasibility study of a CubeSat capturing the AKM surface of a larger piece of debris with a robotic clamp and alter its orbit.

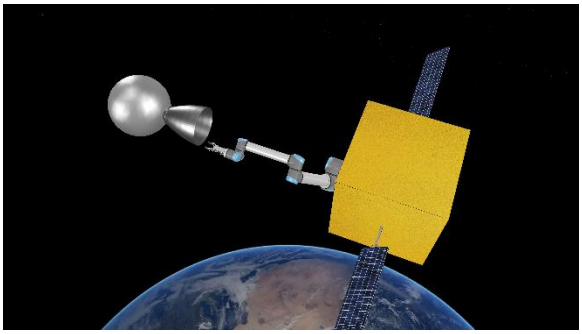

Figure 1: Simulated scene of a chasing spacecraft attempting to capture an Apogee Kick Motor.

A common element of these works is that they suggest capturing various parts of the satellite, to *mechanically restrain* it. They require specialised grippers, designed to capture only that particular spacecraft part. In terrestrial robotics, the field of *grasp synthesis* has enabled robots efficiently grasp objects of various shapes, by analysing the grasp mechanics and leverage visual input and learning. And while there have been numerous proposed robotic hands for orbital applications [12-14], a limited number of works demonstrate capabilities of intelligent, dexterous grasping and adjustability to new targets. In [15] the authors presented the grasping process of Robonaut2, based on *object affordances* i.e., connections between object, hand

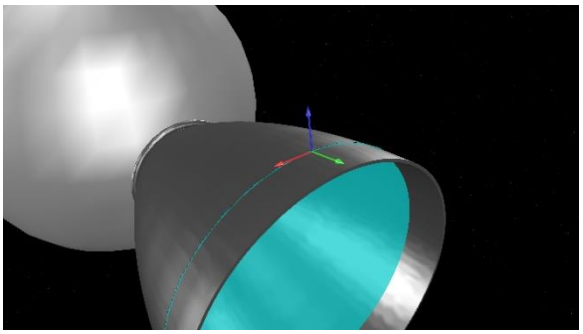

Figure 2: A grasping point located on the the AKM nozzle. The curvature along the y-axis (green arrow) is $k_{b2} = 0$. The curvature along the x-axis (red arrow) is $k_{b1} = {}^{1}/_{r}$, where r is the radius of the cross-section circle that intersects with the point (shown as a light blue disc).

configurations, and associated actions. Our recent work has shown the synthesis of grasping points on the surface of an AKM from a 3D point cloud [16].

A crucial property in robotic grasping is grasp stability i.e. the ability of the fingers to maintain and return to the initial contact point in the presence of external disturbances. Generating stable grasps is similar to mechanically restricting an object. A special case that achieves grasp stability, without grasp synthesis is presented in [17], where the authors introduced a bio-inspired gripper that can latch onto a free-flying object and maintain contact through specialised adhesive pads. This method is excellent for achieving a strong grip, but the hit-and-latch approach leaves limited potential for developing grasp planning with dexterity. This paper presents a method for stable robotic grasp synthesis on an orbital target. Its novelty lies in the attempt to overcome the limitations of the works above by a) introducing grasp stability analysis for orbital targets and achieving the same effect with mechanical grappling b) performing contact point analysis on a surface, that enables straightforward extrapolation to any surface and target, and enabling dexterous planning, and c) using a simple 2-fingered commercial-type gripper for the analysis, instead of specialised equipment. We select the surface of an AKM nozzle as the surface on which we base our analysis, because it is a widely used in orbital robotics, and its curved surface increases the grasp stability.

2 METHODOLOGY

The core of our method is based on the analysis of [18] and [19]. We briefly describe the concepts

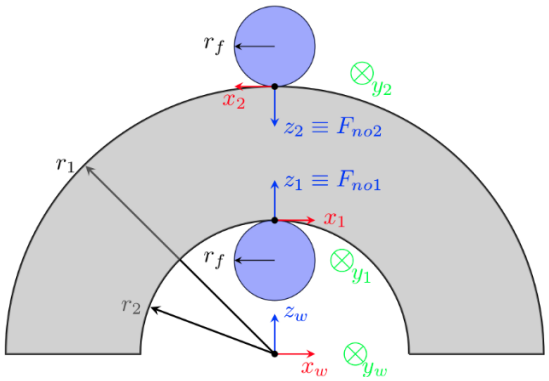

Figure 3: Cross-section of the AKM nozzle and robotic finger. The fingers have radius r_f. The internal AKM radius is noted with r_2 and the external with r_1. In our analysis and real AKMs we have $r_1 \approx r_2 = r$. The fingers apply normal forces of F_{n_1} and F_{n_2}. If $F_{n_1} = F_{n_2}$, the grasp is in equilibrium. O_W is the coordinate frame where we express the Internal Stiffness Matrix K_o and mass matrix M.

developed in these two works for the remainder of the section.

2.1 Surface Curvature

Let S_A be the surface of a robot finger, and S_B a surface patch of the engine nozzle. We define the respective local reference coordinate frames O_A and O_B on each surface. The tangential x and y axes of these frames coincide with the *directions of principal curvature* of each surface, and the z axis is orthogonal. The z-axes of the two surfaces are taken to be colinear, and we let ψ the difference of orientation of z-axes around this common normal. We note with (k_{a1}, k_{a2}) and (k_{b1}, k_{b2}) the *principal curvatures* of each surface, and we define the following curvature matrices:

$$L_A = \begin{pmatrix} -k_{a1} & 0 \\ 0 & -k_{a2} \end{pmatrix} \quad (1)$$

$$L_B = \begin{pmatrix} cos\psi & sin\psi \\ sin\psi & cos\psi \end{pmatrix} \begin{pmatrix} -k_{b1} & 0 \\ 0 & -k_{b2} \end{pmatrix} \begin{pmatrix} cos\psi & sin\psi \\ sin\psi & cos\psi \end{pmatrix} \quad (2)$$

We model the robot fingers as spheres of radius r_f .For each finger i, we have ${}^{i}k_{a1} = {}^{i}k_{a2} = {}^{1}/_{r_f}$. The surface of the engine nozzle can be modeled as a cone. One direction of the nozzle surface is planar, and the perpendicular direction is curved with a variable radius r (blue disk radius in Fig. 2). By

varying the values of ψ, r_f and r, we can analyse the effect of different finger sizes on the grasp stability on different areas of the engine nozzle, under rotations. As such, the principal curvatures of a point on the nozzle surface are $k_{b1} = 1/r$ (aligned with the red axis of Fig. 2, $k_{b2} = 0$ (aligned with the green axis of Fig. 2).

2.2 Intrinsic Stiffness Matrix in Weightlessness

We base our stability analysis around the *Intrinsic Stiffness Matrix* (ISM) as developed in [18]. The ISM characterises the grasp stability based on the grasp geometry, applied forces, finger and object local curvatures, and friction. It assumes that the finger mechanisms are non-compliant. For simplicity we assume that the fingers are non-compliant. This enables us to draw conclusions about the stability of the underlying grasp geometry, ignoring the effect of the finger compliance and structure, and providing a solution that is mechanism independent.

Given a set of finger contact points on an object's surface, the ISM relates the variation of the total applied wrench on the object from all fingers, to the variation of the object displacement. This corresponds in the second-order change in the grasp's potential energy:

$$\Delta\vec{F} = -K_o \Delta\vec{x}_o \tag{3}$$

where K_o is the 6×6 ISM, $\vec{F} \in R^6$ is the total applied wrench on the object from all contacts, and $\vec{x}_o \in R^6$ is the object translation and rotation vector, expressed in a global reference frame O_w. For grasps in force equilibrium, K_o is symmetric.

Eq. (3) applies also on each contact, relating the variation in applied wrench from one finger, to the total displacement of the object. In this case, the *contact stiffness matrix* K_c is a function of the combined local curvatures of the finger and surface, the applied force, and the frictional and elastic properties of the contact. K_c is given in Eq. (4) (next page). k_t is the shear stiffness constant, k_θ the torsional stiffness constant, and k_n the compressive stiffness constant. The stiffness constants are functions of the fingertip's material shear and elasticity moduli, and the contact cross-section dimensions [20]. M_o is the torsional moment on each finger that holds the object at equilibrium. F_{to} is the tangential force on each contact that result from friction. The tangential force needs to be within the *friction cone* of the contact to prevent contact sliding. Additionally, $\Lambda = \begin{pmatrix} 0 & 1 \\ -1 & 0 \end{pmatrix}$. Each finger applies a normal force F_{no} on the finger-surface contact point. After calculating the contact stiffness matrix K_{c_i} for each contact, the ISM is:

$$K_o = \sum_{i=1}^{N} (T_i^T K_{c_i} T_i + T_{mg}^T K_{c_{mg}} T_{mg}) \tag{5}$$

where N is the number of contact points on the object, T_i is a transformation matrix from the contact coordinate frame O_i to the reference frame O_w and T_{mg} is a transformation matrix from the object's centre of mass to O_w. $K_{c_{mg}}$ is a stiffness matrix for the gravity

force. A change in the object's motion does not alter the gravity force, but it moves the coordinate frame of the object's centre of mass, resulting in variation of the applied toque from the fingers.

$K_{c_{mg}}$ encodes this change in torque to the object displacement. In orbit, we can assume $g = 0\ m/s^2$, and so the gravity force does not affect the intrinsic stiffness of the grasp. This results in $K_{c_{mg}} = 0_{6\times6}$ and Eq. (5) becomes:

$$K_o = \sum_{i=1}^{N} (T_i^T K_{c_i} T_i) \tag{6}$$

Eq. (6) is the ISM used in this paper.

2.3 Grasp Stability Criterion

When the robot fingers are non-compliant, the stability of the grasp is given by examining the eigenvalues of the ISM. If K_o is positive-definite, the grasp is *asymptotically stable*, and the eigenvalues of K_o are all positive. If one eigenvalue is negative the grasp is *unstable*, and if there are zero eigenvalues the grasp is *marginally stable*, and higher order motion analysis of the contacts is required. As mentioned, a reference coordinate frame O_w is required for the calculation of K_o. As described in [19] the eigendecomposition of K_o is not invariant to changes in this reference frame. The *value* of the eigenvalues of K_o changes with the choice of O_w, although their *sign* remains the same. The eigenvalues of K_o have physical units, and they are not invariant to change in the physical unit

$$K_c = \begin{pmatrix} F_{no}L_A(L_A+L_B)^{-1}L_B + k_t I_{2\times1} & 0_{2\times1} & -F_{no}L_A(L_A+L_B)^{-1}\Lambda & 0_{2\times1} \\ 0_{1\times2} & k_n & 0_{1\times2} & 0 \\ (M_oL_A - F_{no})\Lambda(L_A+L_B)^{-1}L_B & \Lambda F_{to} & (F_{no}\Lambda - M_oL_A)(L_A+L_B)^{-1}\Lambda & 0_{2\times1} \\ F_{to}^T\Lambda & 0 & 0_{1\times2} & k_\theta \end{pmatrix} \quad (4)$$

representation. Instead, a measure for grasp stability based on the generalised eigendecomposition of K_o, and a 6×6 matrix M was developed in [19]. The eigenvalues of $M^{-1}K_o$ are positive definite if and only if M and K_o are positive definite. The selection of M is arbitrary, but the use of the object's mass matrix acts as a stability metric with *kinetic energy* information. If the mass matrix M is expressed in the same frame with K_o (O_w), the eigendecomposition makes the eigenvalues of $M^{-1}K_o$ dimensionless, and invariant to where O_w is located on the object. The eigenvalues are then ideal for qualitative analysis of stability. A good stability measure is to compare the *minimum* eigenvalues of multiple grasping configurations (i.e. multiple K_o and one M), and the grasp with larger minimum eigenvalue is stabler. This metric is also useful for determining the stability of a single grasp on objects with various mass distributions (i.e. one K_o and multiple M). We use the above analysis on the surface of an engine's nozzle. We gradually build K_o from the geometry of a robot grasping the engine cone with 2 fingers (Fig. 3). We use the mass matrix of the target in the minimum-eigenvalue stability criterion. In reality, the mass matrix of the target may not be accurately known in advance, but we nevertheless test with a range of mass matrices to assess the stability limits of the proposed algorithm.

3 EXPERIMENTS

We consider a space debris removal scenario as test case. A chasing spacecraft captures a spent upper rocket stage. The rocket stage has been modelled after the Orbital ATK STAR-24C AKM, used in real launches [21]. We selected this target for its simple geometry that enables easier modelling in a simulator. We define a *nominal case* of a chasing spacecraft capturing target. This nominal case has predefined values for the target dimensions and inertial parameters, and the chaser inertial parameters, finger radii, applied force, and ψ displacement angle (Table I.) We evaluate the grasp stability in two ways. First, we conduct a numerical evaluation to test how variations of the grasping parameters affect the stability. Second, we test the nominal scenario using the V-REP simulator, by having the robot executing a capture-and-pull task and measuring the finger slippage.

Parameter	Nominal Value
Nozzle radius r	0.38 (m)
Finger radius r_f	0.038 (m)
Nominal Force F_n	200 (N)
ψ angle	0°
Target mass m	19.69 (kg)

Table I: Parameters for the nominal test case.

3.1 Numerical Evaluation

We propose the following evaluation steps: At first, we evaluate whether the nominal test case yields a stable grasp. We then evaluate the nominal test case again, but for the special case of planar fingers, i.e. $r_f \to \infty$. Most commercial robotic grippers use planar fingers, so we can evaluate the performance of existing gripping technologies for this task. Finally, we change the parameters of the nominal test case, one at a time, within a predefined range.

For the grasp stability criterion, we need the mass matrix of the target, expressed to the same coordinate frame as the ISM. We model the inertia tensor as the combination of a hollow sphere with a conical part attached. The sphere and cone are considered to have uniform density, and their respective masses and dimensions are found from the STAR-24C product manual [22]. The inertia tensor is then expressed to the same coordinate frame O_W as the ISM of the grasp, as per Fig. 3. The frame O_W is selected at the centre of the nozzle exit diameter, at the edge of the total structure. The grasp is located at an offset $(0,0,r)$ w.r.t. O_W, and so for each finger we have $dx = dy = 0$and $dz_1 = dz_2 = r$.

We construct the ISM K_o by substituting the necessary parameters and transformations to Eq. (6). We consider frictionless contacts, which results in $F_{to} = 0$ and $M_o = k_t = k_\theta = 0$. Frictionless assumption enables the assessment of the worst-case scenario [18]. The remaining stiffness constants were modelled with the moduli of aluminium. We

Finger Type	Minimum Eigenvalue
Round Fingertips ($r_f = 0.038$ m)	5.41
Planar Fingertips ($r_f \to \infty$)	0

Table II: The nominal test case stability evaluation.

calculate the minimum eigenvalue of $M^{-1}K_o$. The results are shown in Table II. The spherical fingers yield a more stable grasp, and the planar grasp is marginally stable, as in terrestrial robotics [23].

The next step is to evaluate the stability as a function of the radius of the nozzle r, the radius of the finger r_f, the applied force by each finger F_n, the finger-object angle ψ and the total mass of the target m. As the values of the stiffness constants are typically in the magnitude of 10^6, it was found that they drive the 3rd and 6th eigenvalue at very high values. Their variation is not enough to compromise the grasp stability, and so they are not presented in the numerical analysis. The parameter ranges are shown in Table III. The results are shown in Fig. 4. The nominal test case yields a stable grasp with a large variation margin for all parameters before stability is compromised. In Fig. 4a, larger engine nozzles tend to destabilise the grasp when r_f remains the same. In Fig. 4b the grasp stability increases as r_f increases, as r remains constant. When $r/r_f = 1$, the grasp has the highest stability, but past that point it becomes unstable, and then it asymptotically approaches zero. As a result, the *ratio* of nozzle-to-finger radii r/r_f is a useful design parameter for capturing a spacecraft's nozzle.

Parameter	Minimum Value	Maximum Value
r (m)	0.1	1.2
r_f (m)	0.02	0.15
F_n (N)	10	500
ψ (deg)	0	360
m (kg)	5	200

Table III: Limits for the numerical evaluation.

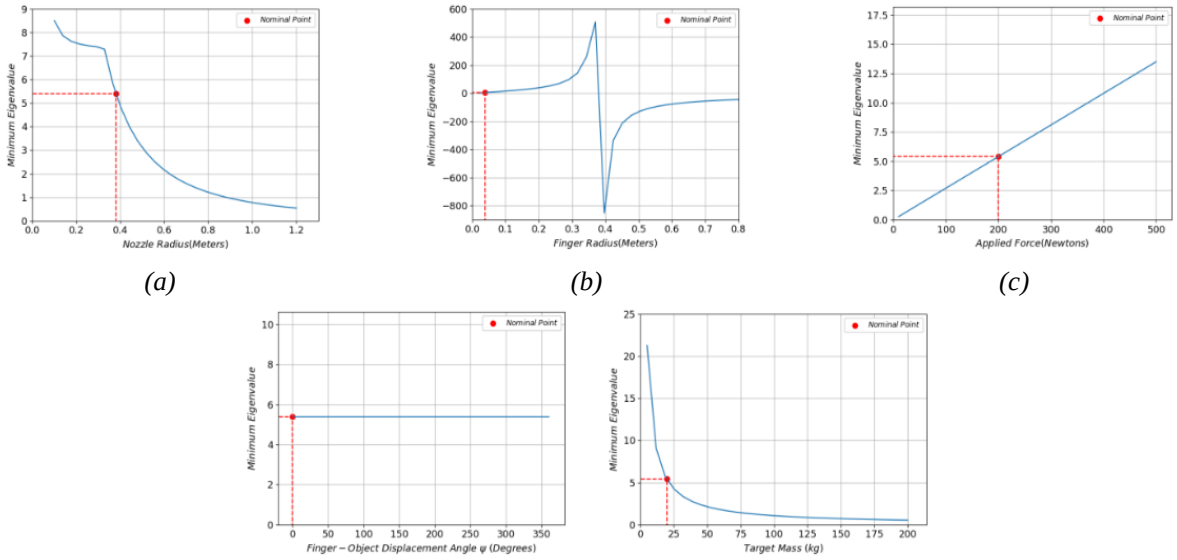

(a) *(b)* *(c)* *(d)* *(e)*

Figure 2: Numerical evaluation results of the nominal test case, when each grasping parameter varies. (a) Nozzle radius. (b) Finger radius (c) Normal force (d) ψ angle (e) Target mass.

The curve of the applied force (Fig. 4c) shows an intuitive behaviour. The grasp is stable as the applying force increases. Where friction is present, an increase of the normal force results in the increase of the tangential force limit required for the object to slide from the grasp, further increasing the stability. The ψ angle (Fig. 4d) corresponds to the relative rotation of the finger and the grasping surface during contact. As the finger is radially symmetric, the combined curvature is not affected by this rotation, and the ψ angle has no effect on stability. We used a complete rotation (0^o - 360^o) for the numerical analysis, but for a real robot the ψ angle would be limited by the gripper reaching capabilities. Finally,

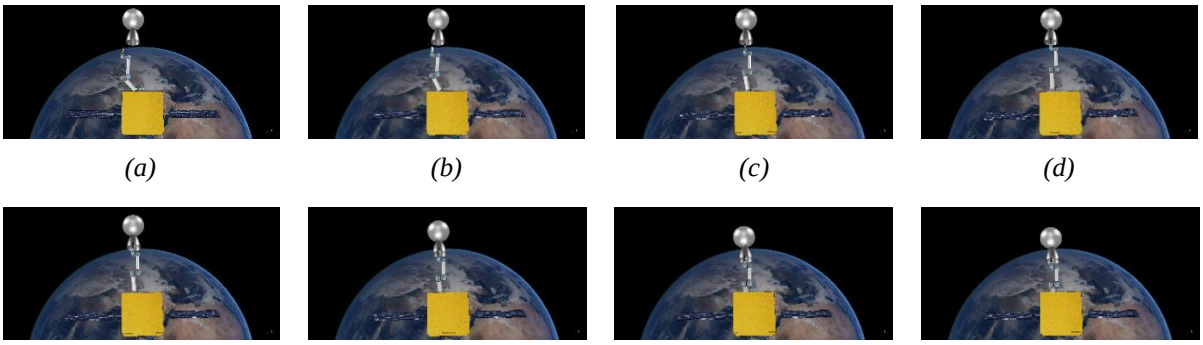

(a) (b) (c) (d)

(e) (f) (g) (h)

Figure 3: Time instances of the AKM grasping and pulling simulation. (a) t=0 sec (b) t=35 sec (c) t=70 sec (d) t=105 sec (e) t=140 sec (f) t=175 sec (g) t=210 sec (h) t=245 sec

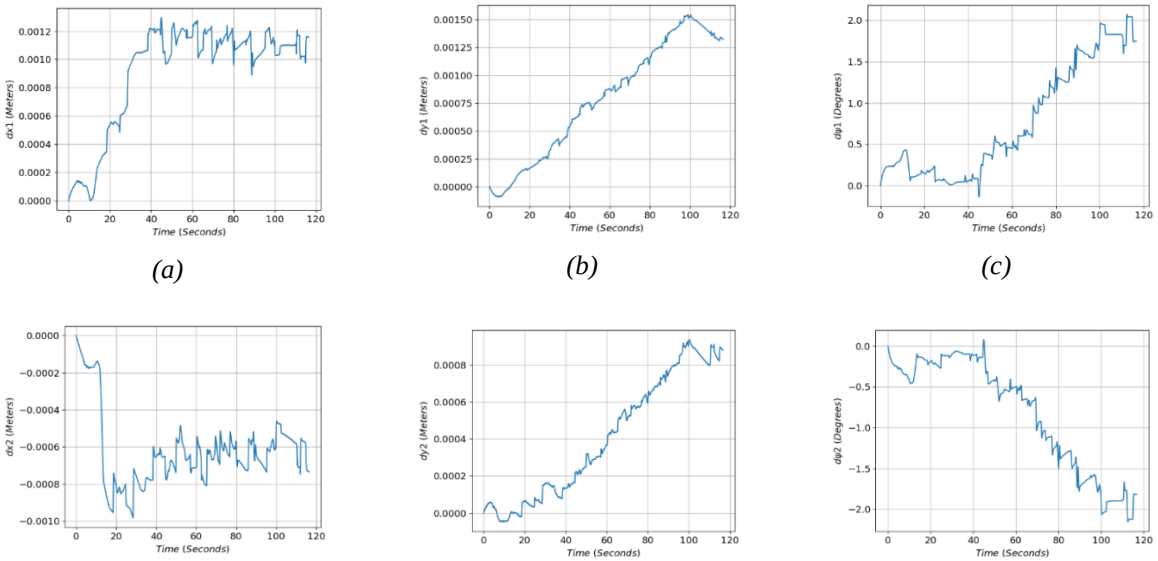

(a) (b) (c)

(d) (e) (f)

Figure 6: Simulation measurements of the fingers' slippage. (a-c) x tangential, y tangential, and rotational slippage for the left finger. (d-f) x tangential, y tangential, and rotational slippage for the left finger.

the mass-stability curve (Fig. 4e) shows that massive objects are difficult to manipulate, and the inertial forces moving them would reflect higher disturbance forces at the contact points.

3.2 Simulation

To further test the grasp stability of the nominal case, we setup a simulation of a capturing task. We use the V-REP simulator to define a weightless scene, where a spacecraft with a robot manipulator and 2-fingered gripper attempt to grasp a STAR-24C motor (Fig. 1).

The simulation was set based on the nominal case parameters of Table I. The STAR-24C motor is modelled with the real dimensions, mass and radius $r = 0.38$ m [22]. The chasing spacecraft has a mass of 500 kg, and the inertial parameters were calculated as per the numerical analysis. The gripper was augmented with rounded fingertips, with $r_f = 0.038$ m. The friction coefficient of the finger-nozzle contact point is $\mu = 1.6$, which corresponds to the friction coefficient of aluminium-aluminium dry contact in vacuum [24]. In reality, the friction coefficient would also be affected by other factors (temperature, wear and residue on the motor after ignition ea.).

The robot reaches a grasping point on the AKM, grasps the object without finger compliance, and applies the nominal force of $F_n = 200$ N. The robot then slowly pulls the object towards the chaser, for a total pulling distance of 0.5 m. An execution of the

task is shown in Fig. 5. The base of chasing spacecraft is left *free-flying* i.e. it is not controlled to compensate for changes in attitude that result from robot-base motion coupling. The lack of compliance in grasping and the lack of base were deliberately selected because they introduce *additional* disturbances and enable drawing conclusions about the stability based on a worst-case performance.

During the grasp execution and the pulling operation, we record the contact-finger displacements on the x_1, y_1,x_2 and y_2 axes, and orientation displacement angle along the axes z_1 and z_2 (Fig. 3). This displacement angle corresponds to the ψ angle. The results are shown in Fig. 6. For a pulling distance of 0.5 m in a little less than 120 sec, the maximum displacements vertical to the motion direction for both fingers (Figs. 6a and 6d) are 1.3 mm for finger 1 and 0.97 mm for finger 2. The maximum displacements parallel to the motion direction are 1.6 mm for finger 1 and 0.9 mm for finger 2. The displacement value of ψ angle is slightly over 2º for each finger, and they follow the same profile with inverse sign. The figures indicate that the robotic grasp shows a stable performance during the task execution.

4 DISCUSSION

We performed stability analysis of grasping an apogee kick motor on orbit in both quantitative and qualitative ways. The results of the numerical analysis show the quantitative behaviour of the grasp over changes in the grasping parameters. The outcome of this analysis can be used for designing stabler orbital grasping algorithms. The simulation test was designed for a qualitative analysis of the orbital grasping task. The results suggest that the grasp is indeed very stable, as small displacement errors are observed. Finger 1 shows a slightly less stable behaviour with larger displacements. This can be attributed to the fact that, as mentioned, grasping concave surfaces (underlying surface of finger 2) offers increased stability over convex surfaces (underlying surface of finger 1). Overall, both tests demonstrate the plausibility of a simple robotic gripper to stably capture a piece of space debris.

5 CONCLUSION

In this paper we presented a novel approach of capturing a spent AKM by employing stable grasp synthesis. A next step for the continuation of this work is the use of a gravity-offload testbed for robotic operations, to confirm the method in an emulator a microgravity environment. The underlying contact analysis can be extended to other targets for on-orbit servicing and debris removal. The usage of dexterous multifingered robotic hands can also enrich the synthesis process. The dynamics of the target and chasing spacecraft can be combined with grasp synthesis for performing motion planning. Finally, compliant control methods can be implemented to ensure minimum target displacement.

Acknowledgement

The work presented has been funded by UKRI/UKSA FAIR-SPACE Hub project (EP/R026092/1), Industry Strategic Challenge Fund.

References

[1] Wenzel W., Palazzetti R., Yan X. T., and Bartsch S. (2017) Mechanical, thermal, data and power transfer types for robotic space interfaces for orbital and planetary missions - A technical review. *Proceedings of the Symposium on Advanced Space Technologies in Robotics and Automation*.

[2] Shan M., Guo J., and Gill E. (2016) Review and comparison of active space debris capturing and removal methods. *Progress in Aerospace Sciences*, 80:18–32, 2016.

[3] Inaba N. and Oda M. (2000) Autonomous Satellite Capture by a Space Robot. *Proceedings of IEEE International Conference on Robotics and Automation*, 2:1169–1174.

[4] Park I-W., Smith T., Sanchez H., Wong S.W., Piacenza P., and Ciocarlie M. (2017) Developing a 3-dof compliant perching arm for a free-flying robot on the international space station. *Proceedings of IEEE International Conference on Advanced Intelligent Mechatronics*, pages 1135– 1141.

[5] Wieser M., Richard H., Hausmann G., Meyer J-C., Jaekel S., Lavagna M., and Biesbroek R. (2015) E. deorbit mission: OHB debris removal concepts. *Proceedings of Symposium on Advanced Space Technologies in Robotics and Automation*.

[6] Ratti J. (2015) Launch adapter ring (LAR) capture tool: Enabling space robotic servicing. *In Workshop of IEEE International Conference on Robotics and Automation*.

[7] Hirano D., Kato H., and Tanishima N. (2017) Caging-Based Grasp With Flexible Manipulation For Robust Capture Of A Free-Floating Target. *Proceedings of IEEE International Conference on Robotics and Automation*, pages 5480–5486.

[8] Yoshida K. and Nakanishi H. (2003) Impedance matching in capturing a satellite by a space robot. *Proceedings of IEEE/RSJ International Conference on Intelligent Robots and Systems*, 4:3059–3064.

[9] Hirzinger G., Landzettel K., Brunner B., Fischer M., Preusche C., Reintsema D., Albu-Schäffer A., Schreiber G., and Steinmetz B. M. (2004) DLR's robotics technologies for on-orbit servicing. *Advanced Robotics*, 18(2):139–174.

[10] Hays A.B, Tchoryk P. Jr., Pavlich J. C., Ritter G. A., and Wassick G. J. (2004) Advancements in design of an autonomous satellite docking system. *Spacecraft Platforms and Infrastructure*, 5419:107–118.

[11] McCormick R., Austin A., Wehage K., Backus S., Miller R., Leith J., Bradley B., Durham P., and Mukherjee R. (2018) REMORA CubeSat for large debris rendezvous, attachment, tracking, and collision avoidance. *Proceedings of IEEE Aerospace Conference*, pages 1–13.

[12] Rubinger B., Brousseau M., Lymer J., Gosselin C., Laliberté T., and Piedboeuf J-C. (2002) A Novel Robotic Hand-SARAH For Operations on the International Space Station. Proceedings of Advanced Space Technologies for Robotics and Automation, (1):1–8.

[13] Chalon M., Maier M., Bertleff W., Beyer A., Bayer R., Friedl W., Neugebauer P., Obermeier T., Sedlmayr H.-J., Seitz N., and Stemmer A. (2015) Spacehand: A Multi-Fingered Robotic Hand for Space. *Proceedings of Symposium on Advanced Space Technologies in Robotics and Automation*, pages 1–8.

[14] Bridgwater L. B., Ihrke C. A., Diftler M. A., Abdallah M. E., Radford N. A., Rogers J. M., Yayathi S., Askew R. S., and Linn D. M. (2012) The Robonaut 2 Hand - Designed To Do Work With Tools. *Proceedings of IEEE International Conference on Robotics and Automation*, pages 3425–3430.

[15] Farrell L., Strawser P., Hambuchen K., Baker W., and Badger J.. Supervisory control of a humanoid robot in microgravity for manipulation tasks. (2017) *Proceedings of IEEE International Conference on Intelligent Robots and Systems*, pages 3797–3802.

[16] Mavrakis N. and Gao Y. (2019) Visually guided robot grasping of a spacecraft's apogee kick motor. *Proceedings of the Symposium on Advanced Space Technologies in Robotics and Automation*.

[17] Jiang H., Hawkes W. W., Fuller C., Estrada M. A., Suresh S. A., Abcouwer N., Han A. K., Wang S., Ploch C. J., Parness A., et al (2017) A robotic device using gecko inspired adhesives can grasp and manipulate large objects in microgravity. *Science Robotics*, 2(7):eaan4545.

[18] Howard W. S. and Kumar V.. On the Stability of Grasped Objects. (1996) *IEEE Transactions on Robotics*, 12(6):904–917.

[19] Bruyninckx H., Demeyt S., and Kumar V. (1998) Generalized Stability Of Compliant Grasps. *Proceedings of IEEE International Conference on Robotics and Automation*, 3:2396–2402.

[20] Cutkosky M. R and Wright P. K. (1986) Friction, stability and the design of robotic fingers. *The International Journal of Robotics Research*, 5(4):20–37.

[21] Boggess A., Carr F. A., Evans D. C., Fischel D., Freeman H. R., Fuechsel C. F., Klinglesmith D. A., Krueger V. L., Longanecker G. W., Moore J. V., et al. (1978) The IUE spacecraft and instrumentation. *Nature*, 275(5679): 372–377.

[22] Alliant Techsystems Inc. (2008) ATK space propulsion products catalogue.

[23] Funahashi Y., Yamada T., Tate M., and Suzuki Y. Grasp Stability Analysis Considering The Curvatures At Contact Points. (1996) *Proceedings of IEEE International Conference on Robotics and Automation*, 4(April):3040–3046.

[24] Deulin E. A., Mikhailov V. P, Panfilov Y. V., and Nevshupa R. A. (2010) Mechanics and physics of precise vacuum mechanisms, volume 91. *Springer*.